DARK MATTER TOMOGRAPHY

TONY TYSON
Bell Labs, Lucent Technologies
Murray Hill, NJ 07974

SLAC Summer Institute, August 1998
Stanford Linear Accelerator Center

LECTURE 1

1. COSMOLOGICAL MOTIVATION

STANDARD COSMOLOGY (1980's):

$$\Omega = 1$$

$$\Lambda = 0$$

$$\Omega_{matter} \approx \Omega_{WIMP,axion} \sim 1 >> \Omega_{baryon}$$

CURRENT MODEL:

$$\Omega_{matter} \approx \Omega_{WIMP,axion} \approx 0.2 - 0.4 >> \Omega_{baryon}$$

Either $\Omega \neq 1$ or $\Lambda \neq 0$

i.e. either $\Omega = \Omega_{matter} < 1$, or $\Omega_{matter} + \Omega_\Lambda = 1$

Either way, we are led to new physics. The nature and distribution of dark matter plays a central role.

Most of the matter in the Universe is of unknown form and dark: Stars (and related material) contribute a tiny fraction of the critical density, $\Omega_{\rm lum} = 0.003 \pm 0.001 h^{-1} \sim 0.004$, while the amount of matter known to be present from its gravitational effects contributes around 100 times this amount, $\Omega_{matter} = 0.3 \pm 0.1$. The gravitational mass of dark matter is needed to hold together everything large in the Universe – galaxies, clusters of galaxies, and superclusters. A variety of methods for determining the amount of matter all seem to

converge on $\Omega_{matter} \sim 1/3$; they include measurements of the masses of clusters of galaxies and the peculiar motions of galaxies. Finally, the theory of big-bang nucleosynthesis and the recently measured primeval abundance of deuterium (Burles & Tytler 1997) tightly constrain the baryon density: $\Omega_{baryon} = (0.02 \pm 0.002)h^{-2} \sim 0.05$. The factor of ten discrepancy between this number and dynamical and lensing measurements of the matter density is evidence for nonbaryonic dark matter.

2. DARK MATTER TIMELINE

Dark matter leads to large scale structure formation, via gravitational instability. How much is there and where is it?

Zwicky (Phys. Rev. 1937, 51, 290). [knew it all]

Rubin & Ford found non-Keplerian orbits for stars and gas in spiral galaxies, implying enclosed mass rising $\sim r$, and dark massive halos.

Press & Gunn (1973) showed that $\Omega \sim 1$ in dark compact objects would produce too many "Einstein rings."

First cosmic mirage discovered. Walsh, etal (1979) find a doubly lensed quasar Q0957+561. The lens: a foreground galaxy with massive dark halo.

In the 1980's it was realized that dominant mass dark halos were good: they stabilize galaxy stellar disks.

Galaxy dark matter halos: Big, but how big?

Clusters of galaxies: Even bigger. (10^{25} cm)

Two kinds of dark matter, two problems. Hot and Cold. Baryonic and non-baryonic. Most of the baryonic matter is dark. Most of the dark matter is non-baryonic.

Have we found it all?

A key problem with viewing our Universe: we've been looking under lamp-posts.

Need to weigh space.

3. CLUSTERS: THE PLACE TO BE AND BE SEEN

Our view of the Universe traditionally has been baryon-biased: we see or detect luminous objects. Yet for the past 15 years it has become more certain that the Universe is dominated by non-baryonic dark matter (Blumenthal etal 1984; Peebles 1993). Nevertheless, luminous objects – through their dynamics – may supply indirect estimates of the underlying mass.

As overdense regions in the Universe grow, some of them become sufficiently overdense that they "freeze out"; inside some radius they overcome the expansion of the Universe. As their density rises into the non-linear regime their internal density fluctuation spectrum bears little resemblance to the primeval spectrum. However, it is hoped that at least their matter *content* is representative of the Universe. It is probably too much to hope that their mass-to-light ratio is also representative. Nevertheless, traditionally they have been found via their radiation (optical light or X-ray). Until recently, the masses of galaxy clusters have played a dominant role in our understanding of dark matter problems.

Cluster masses can be estimated by three different techniques which, on scales of 1 Mpc, give consistent results. The first, which dates back to Fritz Zwicky (1935), uses the measured velocities of cluster galaxies and the virial theorem to determine the total mass (i.e., $KE_{\rm gal} \simeq |PE_{\rm gal}|/2$). Assuming further that the mass-to-light ratio of clusters is the same as the mean mass-to-light ratio in the Universe, Carlberg etal. (1996) combine their measurement of the dispersion of velocities of hundreds of galaxies in several clusters find with a measurement of the mean light density to arrive at an estimate of the mean mass density: $\Omega_M \approx 0.25$. If clusters have more luminosity per mass than average, this technique would underestimate Ω_M.

The second method uses the temperature of the hot X-ray emitting intracluster gas and the virial theorem to arrive at the total mass. In this method, one must assume that the hot gas is pressure supported and in equilibrium. The density and temperature profiles of the hot gas must also be obtained. Usually temperature is not mapped, so isothermality is assumed when inverting flux maps to get the potential.

The third and most direct method is using the gravitational lensing effects of the cluster on much more distant galaxies. Close to the cluster center, lensing is strong enough to produce multiple images; farther out, lensing distorts the shape of distant galaxies. The lensing method allows the cluster (surface) mass density to be mapped directly. [In the following I will use h, the Hubble constant in units of 100 km s^{-1} Mpc^{-1}. Recently h has been measured to 10% accuracy, $h = 0.67 \pm 0.07$ (Garnavich etal 1998).]

X-ray measurements more easily determine the amount of hot, intracluster gas; most of the baryonic mass in a cluster resides here rather than in the mass of individual galaxies (this fact is also confirmed by lensing measurements). If we can assume that clusters are

fair samples of matter in the Universe, we can use baryogenesis to get an indirect estimate of Ω_M. Together with the total cluster mass, the ratio of baryonic mass to total mass can be determined; a compilation of the existing data (Evrard, etal 1996) gives $M_B/M_{\rm TOT} = (0.07 \pm 0.007)h^{-3/2} \sim 0.15$. Invoking the "fair sample" ansatz $\Omega_B/\Omega_M = M_B/M_{\rm TOT}$, the accurate BBN determination of Ω_B can be used to infer: $\Omega_M = (0.3 \pm 0.05)h^{-1/2} \sim 0.4$.

Traditional methods of estimating total mass of clusters are indirect: mass estimators based on kinematics or X-ray flux maps involve models of orbits or the state of the hot gas, leading to potential systematics in the derived gravitational potential. While the dynamical evidence for dark matter is strong on scales from galaxies to superclusters of galaxies, it is worthwhile exploring independent observational techniques which do not rest on assumptions about the orbits of test particles.

4. INTRODUCTION TO LENSING

Gravitational lens distortion of background galaxies enables calibrated measurements of the distribution of dark matter in the Universe. This lens phenomenon is most naturally divided into two broad classes: strong lensing and weak lensing. In weak lensing the gravitational deflection angles are very small and single sources produce single (but distorted) images. In strong lensing, sources appear highly distorted and can form multiple images. Whether a given source is weakly or strongly lensed depends on the impact parameter of the ray: whether its image appears outside or inside the critical "Einstein" radius. For an excellent tutorial, see Narayan & Bartelmann, astro-ph/9606001.

The large number of potential sources in the wide area outside the critical radius of a foreground lens offers the possibility of statistical tomographic reconstruction of the mass distribution in the outer parts of the lens. This weak gravitational lensing provides a direct measure of mass overdensity on large scales (several kpc to tens of Mpc, depending on the distance and compactness of the lens). Through comparison with large N-body simulations for various cosmogonies, this new window on mass in the Universe constrains the nature of dark matter. For example, light neutrino hot dark matter collapses into large structures first, creating top-down structure formation: deep large potential wells come first, small galaxy-sized masses come last. During decoupling this relativistic (hot) dark matter clusters on large scales but free-streams on small scales, preventing galaxy formation (in the absence of dominant cold dark matter) (White, Frenk & Davis 1983).

Strong lensing analysis constrains the mass distribution in the parts of the lens which exceed the critical density for image splitting. In cases where multiple images of a source are

created by the lens, the details of the position and distortion of these sub-images are highly sensitive to the projected 2-dimensional mass distribution in the lens.

In weak lensing it is necessary to average over the apparent orientation of tens of sources for each resolution element: typically, weak lens statistical inversion uses thousands of "arclets" (distorted background galaxies) over a wide field. The largest source of noise in weak lens inversion of deep optical images is the ellipticity noise of the source population itself. A number of non-parametric algorithms have been developed for inverting the arclets, and regularized approaches tend to avoid edge effects and systematics near the strong lens regime.

Up to a constant sheet of mass, lensing inversion can be calibrated and has no adjustable parameters. Calibration of the mass scale can be done both through simulations and via observation of a mass standard. Realistic simulations of the whole source-lens-atmosphere-detector process, including multiple background galaxy redshift shells, masses for individual cluster galaxies, dark matter lens model, atmospheric seeing, and pixel sampling and sky shot noise, must be performed. "Blank" field Hubble Space Telescope imaging data, together with seeing deconvolved ground-based data, are used to derive the source galaxy angular scales. Strong lensing forms an independent check on weak lensing mass scale calibration. In this first lecture I will outline these parametric mass reconstruction techniques which have been used in strong lensing.

5. THE SOURCES

To 30th magnitude per square arcsecond surface brightness (4×10^{-18} erg sec^{-1} cm^{-2} arcsec^{-2} in 100 nm bandwidth at 450 nm wavelength, or about five photons per minute per galaxy collected with a 4-meter mirror) there are about 50 billion galaxies over the sky. Nature has been particularly kind to us: Since many of the faint galaxies are resolved and are distributed up to high redshifts they may be employed in statistical gravitational lens studies of foreground mass distributions. As we will see, if galaxies were a few times smaller or less luminous in the past, this "cosmic mirage" would be extremely difficult to use. Here are the contents of nature's lensing toolbox: For mass mapping by statistical gravitational lens inversion, the sources must meet several requirements: The sources must have (1) redshifts large compared with the lens, (2) a number density on the sky sufficient to sample the lens shear field on relevant scales, (3) an intrinsic angular diameter larger than the ratio of seeing FWHM to the magnification of the lens, (i.e. we must be able to detect the image distortion) and (4) other properties (blue color and unique surface brightness) enabling efficient separation of the sources from lens and other foreground objects.

The extreme blue colors of the faint galaxies results from thier large look-back times:

we see these young galaxies just forming a generation of hot and UV-bright stars at redshifts of 1–3, so that their UV excess flux is redshifted into the blue. In a redshift-magnitude plot the trend to redshift ~ 1 at 25th B magnitude is clear. A typical galaxy seen at z=1 may be a 0.1 $L^\star$ galaxy, so a survey at 25th magnitude would cover a wide range in redshifts extending from 1–3. For arclet inversion of $z < 0.3$ lenses, the lack of detailed redshift data for each of these sources produces less than a 10% mass scale error. We can do even better: if deep imaging is done in several wavelengths, there is enough low-rez spectral information to supply so-called "photometric redshifts", accurate to $\Delta z = 0.1$, so we can separate galaxies into broad foreground and multiple background redshift bins. This raises the lens inversion signal-to-noise level.

Without luminosity evolution these distant background galaxies would have prohibitively faint surface brightness ($SB \sim (1+z)^{-4}$). Even with their luminosity evolution (brighter earlier), very faint levels of surface brightness must be achieved. This is the most difficult part of this technique, and is why many orbits on HST or many nights on large ground-based telescopes are required per field. At any surface brightness limit, there is a redshift selection function.

Galaxies fainter than 26 B magnitude also cover a wide range of angular scales; typical half-light diameters are 1 arcsecond (Im, etal 1995). The number density of galaxies on the sky vs magnitude is shown in Figure 1. 4-meter class telescopes can image one square degree to a magnitude limit of 26 B (blue) mag and 29 B mag arcsec^{-2} surface brightness in several nights per wave-band.

6. LIGHT BENDING

The path of a photon from a distant source is bent as it passes by the foreground mass (gravitational lens), making the source appear at an altered position (for a good review, see Blandford and Narayan 1992). This light-bending is accompanied by another first-order effect: systematic image distortions. If the background source image is resolved then this image stretching is observable. A galaxy of angular size one arcsecond may appear to be moved by an angle $\beta = 4GM(r)/rc^2$ and distorted into an arc many arcseconds long by sufficient foreground mass $M(r)$ interior to projected radius r. The scattering time is small compared with the period of orbiting test particles, thus avoiding orbit assumptions.

The light deflection is proportional to the mass in the lens and is about two arcsec for a typical galaxy (Turner *et al* 1984). If ϕ is the intrinsic source position in the absence of the lens, the source appears at position θ:

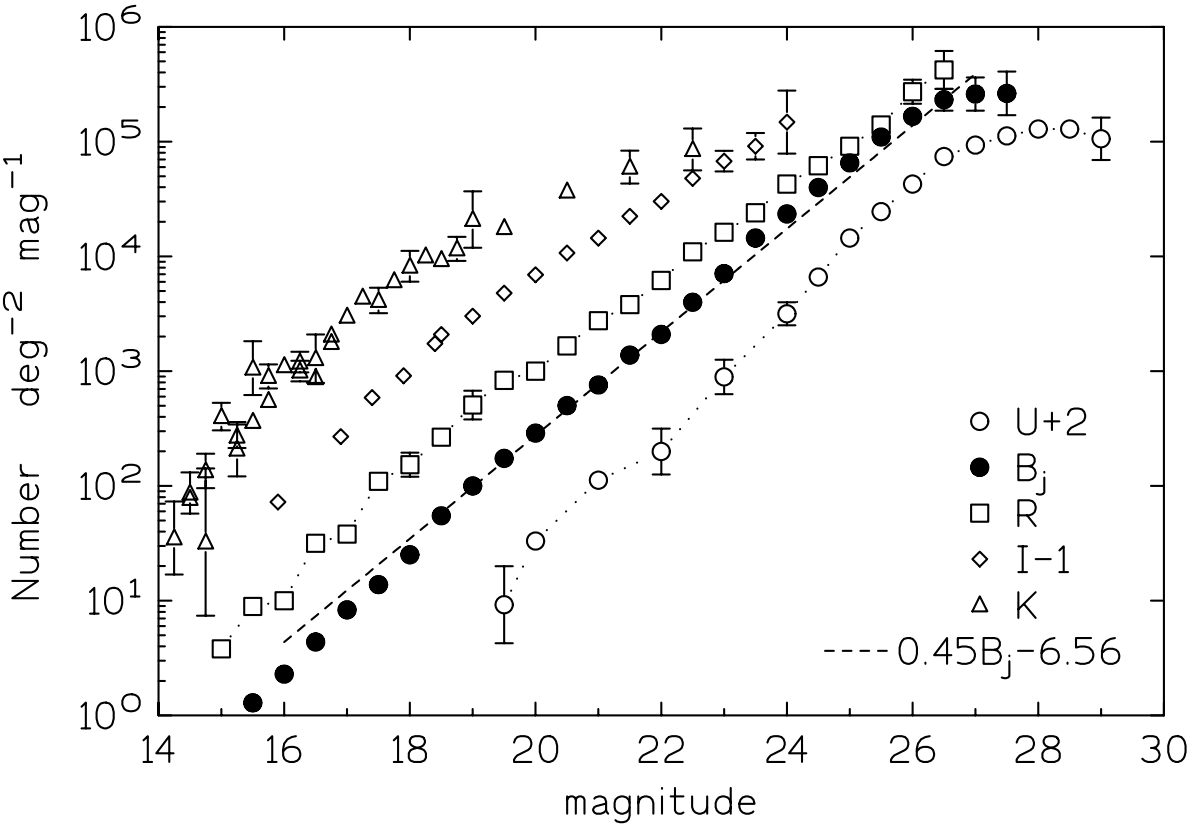

Fig. 1.— *Number density of galaxies (the sources) on the sky, as a function of magnitude (-2.5 log Flux) for several wave-bands, U (360 nm), Bj (450 nm), R (600 nm), I (800 nm) and K (1200 nm). There is a faint galaxy every few arcseconds on the sky, in deep imaging on 4-meter telescopes – sufficient to define the shear field of a foreground gravitational lens.*

$$\vec{\phi} \;=\; \vec{\theta} \;-\; \vec{\delta}(\vec{\theta}), \tag{1}$$

$$\vec{\delta}(\vec{\theta}) \;=\; (D_{LS}/D_S)\;\vec{\beta}(\vec{r}),$$

where r is the impact parameter for the ray at the lens, and D_S and D_{LS} are the observer-source and lens-source angular diameter distances. For a thin lens the light bending angle $\vec{\beta}$ is given in terms of the projected two dimensional mass density Σ:

$$\vec{\beta} \;=\; (4G/c^2) \int d^2u\; \Sigma(\vec{u})\; (\vec{r}-\vec{u})\;/\;\mid \vec{r}-\vec{u}\mid^2 . \tag{2}$$

We would like to invert this relation and solve for Σ(x,y). Since we do not know how the sources were distributed on the sky prior to lensing, this deflection itself is not observable. But its gradient, the shear, is directly observable. In the simple case of a pont mass, $\beta = 4GM/rc^2$, and a source exactly behind the mass appears as an "Einstein ring" image of radius $\theta_E \;=\; (M\;/\;10^{11}\;M_\odot)^{1/2}\;(D\;/\;10^6\;\mathrm{kpc})^{-1/2}$ arcseconds, where D $= D_L\;D_S\;/\;D_{LS}$. If the lens mass is elliptical in shape or has multiple components this circular ring symmetry is broken, so that in nature circular rings are rare. If the source angle ϕ is less than θ_E then multiple images of the source are formed. Galaxy lenses ($M \approx 10^{12}\;M_\odot$) will produce multiple images with separations ≈ 3 arcseconds, while galaxy cluster lenses ($M \approx 10^{14}\;M_\odot$) can produce image separations of one arcminute. In the case of an isothermal distribution of gravitationally bound masses of line-of-sight velocity dispersion σ_v, $\beta(r) = 4\pi(\sigma_v/c)^2$, $\theta_E \;=\; 29\;(\sigma_v\;/\;10^3\;\mathrm{km\;sec}^{-1})^2\;(D_{LS}\;/\;D_S)$ arcseconds. Many clusters have measured velocity dispersions $\approx 10^3$ km sec^{-1}.

6.1. SIMULATION VIDEO

MPG MOVIE of our view, over the next few billion years, of a cluster of galaxies and the effects of its dark matter.

This simulation was made by our group, principally Ayana Holloway. It shows the cluster A1689 as viewed by Earth orbiting space telescopes over the next few billion years; as it moves through the Universe its alignment with the background faint blue galaxies constantly changes. The data for the cluster (the orange bright galaxies) are from the Hubble Space Telescope [we do not show time evolution of the cluster galaxies in their orbits], and the mass model we used in the simulation is one which we are developing via strong lens

parametric techniques. The background galaxies are placed in 6 redshift sheets, out to z = 3. Fainter and bluer galaxies are at higher redshift. Some galaxies just behind the cluster (coded brighter and less blue) are only slightly distorted by the concentration of dark matter. The highest redshift faint galaxies easily form large arcs (perturbed Einstein rings) at larger radii.

In this simulation, the mass distribution is composed of dark matter halos for individual cluster galaxies as well as the dominant diffuse mass of the cluster. This largest mass has a soft core. A non-singular lens mass produces an odd number of images of a background galaxy. When the galaxy is at large projected radius (weak lens regime) it is slightly distorted orthogonal to the radius vector. As the galaxy moves into the critical region it splits into an odd number of images, usually two arcs on opposite sides of the lens and a third, demagnified, image near the center. The details of these images – their parity and magnification – are sensitive to the gradient of the lens mass. For lens mass density exceeding Σ_{crit}, the magnification determinant is negative – the lens-focussed light bundle comes to a focus before reaching Earth; images inside this radius (one of the odd images) appear demagnified and with opposite parity. These faint radial spokes may be seen for many of the background galaxies, and are a sensitive indicator of the size of the soft mass core.

7. TOMOGRAPHIC RECONSTRUCTION OF GALAXY CLUSTER MASS

7.1. STRONG LENS PARAMETRIC MASS MODELS

In cases where portions of the lens exceed critical density, producing multiple images of some sources, it is possible to obtain higher resolution in the mass map by combining weak lens inversion at large radius with the strong lensing constraints in the inner region. One approach is to use a parametric lens model in which multiple mass components are parametrized by their centroid, mass profile, and ellipticity. An iterative approach, regularized by the weak lens inversion solution for the mass at large radius, is then used to obtain a unique solution for the lens mass map at high resolution.

This has the desirable property that the resulting mass map has high resolution in regions of high mass density. In practice we have found that a reliable way of converging to the solution is to demand that the strong lensed sources, when unlensed by the estimated mass distribution in the lens, reconstruct to an identical single image [see Colley, etal 1996], and that this image of the source maps to the observed arcs (and only these arcs!) in the image plane when lensed by this same mass. It is necessary to use the lens *mass* distribution,

rather than the traditional approach of starting with a 2-dimensional lens potential, as non-circular lens potentials can be unphysical in their corresponding mass reconstructions.

As an example, I show a high resolution mass map of the $z = 0.39$ cluster 0024+1654, based on parametric inversion of the associated gravitational lens (Tyson, Kochanski, & Dell'Antonio 1998). This lens creates eight well-resolved sub-images of a background galaxy, seen in deep imaging with the Hubble Space Telescope.

We parametrized the source as 58 smooth disks of light. Each of these disks was characterized by an intensity, a scale radius, and the (x, y) position on the source plane (4 parameters). A source plane resolution of 7 milli-arcseconds per pixel was chosen to allow sufficient evaluations of the model to be done within a reasonable time (12 months), and to allow the model to represent almost all details of the observations. The source is then ray-traced through the lens plane, and the resulting image is compared on a pixel-by-pixel basis with the HST image. We parametrize the mass distribution as a cluster of mass concentrations ("mascons"). Each mascon is based on a power law model ("PL", Schneider et al. 1993) for the mass density $\Sigma(r)$ vs projected radius r, with both an inner core radius and an outer cutoff radius

$$\begin{aligned} \Sigma(x) &= \frac{K_1(1+\alpha x^2)}{(1+x^2)^{2-\alpha}} \qquad x < X_o \\ \Sigma(x) &= K_2 x^{-3} X_o^3 \qquad x \geq X_o, \end{aligned} \tag{1}$$

where $x = r/r_{\rm core}$, $X_o = r_{\rm cutoff}/r_{\rm core}$, and α is the PL model index. ${K_1}^{0.5}$ is proportional to the central line-of-sight velocity dispersion. We build up elliptical mass distributions by superposing a line of overlapping circular mascons. In principle, each mascon is described by 9 parameters. The first four come directly from the equation above (K_1, an inner mass core radius $r_{\rm core}$, an outer mass cutoff $r_{\rm cutoff}$, and the slope of the mass profile α). For elliptical mass distributions, there are three parameters describing the ellipticity (the position angle θ, the length of the line of mascons l_{core}, and the uniformity of the spacing of the mascons along the line). For mass components not associated with optically observed galaxies, the x and y position in the lens plane are also free.

The mass and linear scale sensitivity of this parametric lens inversion technique vary with position in the cluster; cluster mascons projected near a long arc have the effect of their mass distribution highly magnified. For galaxies that are more than about $5''$ from the arcs, only their total mass matters, and we parametrize this by the cutoff radius (because $M \propto r_{\rm cutoff}$). Galaxies farther than about $20''$ from the arcs are parameterized in groups.

In all, the mass and source models are determined by 512 parameters. However, we have over 3800 significantly nonzero (3σ) pixels in the arcs which supply sufficient information.

Because the optical point spread function of the WFPC2 is smaller than one pixel, the signal is nearly uncorrelated even on neighboring pixels; thus, we have many more independent constraints than model parameters. In addition, pixels with no signal serve as constraints, because they prevent the model from putting flux in areas of the image where it should not. The resulting mass model is over-constrained. The optimizer uses simulated annealing and bootstrap resampling to avoid false minima.

As we developed the model, it had enough power to predict the central image, based on the three major arcs, then to correctly predict the multiple subimages near the outer arcs. The galaxy masses in the model were initialized using the Faber-Jackson relation. When the model evolved to a low χ^2, we performed robustness tests by perturbing the position and/or mass of a mascon and observing the reconvergence to the the solution (see Figure 2). Over 2×10^6 models were searched to reach the solution. In addition to the large diffuse mascons, other mascons were added to our fit to allow it to match the complexity of the cluster's mass distribution. Several "dark" galaxies were found.

The vast majority of the DM is *not* associated with the galaxies, and appears as a smooth elliptical distribution centered near the position of the brightest galaxy and elongated in the SE-NW direction. The elongation is in the same direction as that of the X-ray isophotes. This DM not associated with galaxies shows no evidence of infalling massive clumps: other than these two major clumps, we find no dark mascons with total mass greater than $5 \times 10^{12} M_\odot$ (1.5% of the cluster mass), out of the 25 in the fit.

Excluding mass concentrations centered on visible galaxies, more than 98% of the remaining mass is represented by a smooth concentration of dark matter centered near the brightest cluster galaxies, with a 33 h^{-1} kpc *soft core*. The asymmetry in the mass distribution is <3% inside 107 h^{-1} kpc radius. The dark matter distribution we observe in CL0024 is far more smooth, symmetric, and nonsingular than in typical simulated clusters in either $\Omega = 1$ or $\Omega = 0.3$ CDM cosmologies. Integrated to 107 h^{-1} kpc radius, the rest-frame mass to light ratio is $\mathrm{M}/L_V = 238 \pm 16\ h\ (M/L_V)_\odot$, rising with radius (see Figure 3). This translates to a mass-to-light ratio of 400 h now. For scale, we would need around 1200 to get $\Omega_M = 1$.

The mass distribution in CL0024 is remarkably relaxed. If one assumes Gaussian density fluctuations in an $\Omega = 1$ Universe, the fluctuation that seeded CL0024 must have had a very large amplitude quite early (rare) to have become virialized by $z = 0.39$. One is led to consider non-Gaussian fluctuations or $\Omega << 1$. An important open question is whether galaxy cluster formation is still continuing at recent times. That is, do a significant fraction of galaxies fall into a pre-existing deep cluster potential? Given that galaxies are detected at redshifts as high as 4, simple top-down (large scales first) structure formation is ruled out.

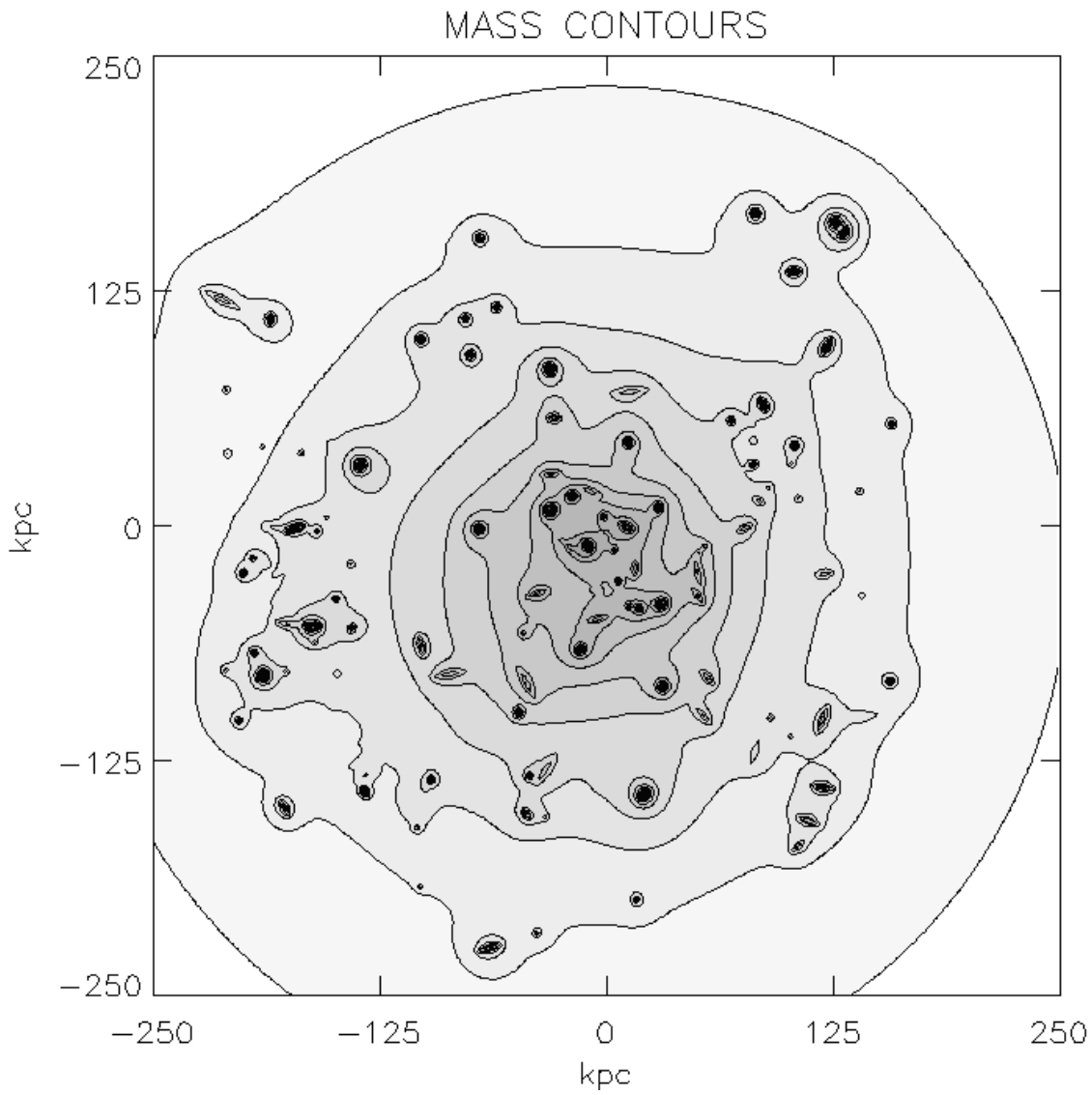

Fig. 2.— *A map of the projected mass density in the redshift 0.4 cluster CL0024+1654, obtained by fitting the observed distorted images of a $z = 1.6$ source galaxy. Dark matter halos of individual galaxies in the cluster are seen, but the major dark matter component is relatively smooth compared with CDM simulations.*

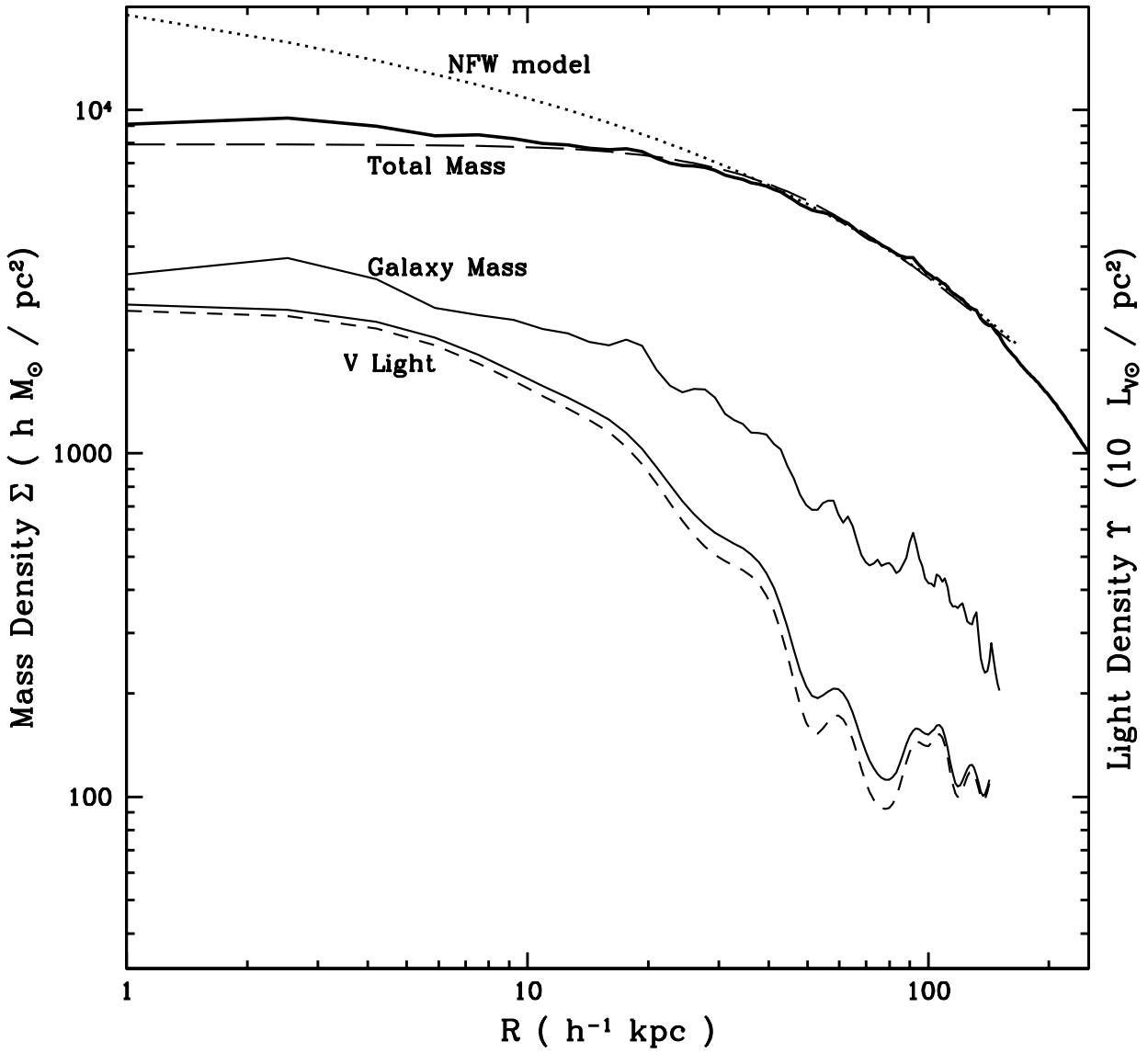

Fig. 3.— *The projected mass density of CL0024 and the projected light density are plotted vs radius. The diffuse dark matter component dominates, and has a soft core. Note also that the mass-to-light ratio rises with radius.*

But there may be several components to the mass-energy of the Universe, and thus multiple contributors to the density profile of clusters.

A key result of this first high resolution mass map is the existence of a 33 h^{-1} kpc soft core. Any possible singularity must be quite small, contributing less than 2×10^{11} $h^{-1} M_{\odot}$ to the total mass within 33 h^{-1} kpc (10% of the mass of one of the central elliptical galaxies). Because cold collisionless particles have no characteristic length scale, the soft core suggests nongravitational interactions. While HDM can produce soft cores, HDM is not consistent with the high density of DM that we find in the individual cluster galaxies. Because of the relatively low X-ray luminosity (0.7 L_X^*), it is very unlikely that this can be attributed to hot gas alone.

This first high resolution mass map of a cluster of galaxies will be useful to compare with future N-body/gas-dynamical simulations. None of the recent simulations show evidence of a soft core, in disagreement with these observations. Indeed, as the resolution of simulations increases from 100 to 30 kpc the central mass becomes more singular (see Syer & White 1998 and references therein).

LECTURE 2

1. STATISTICAL WEAK LENSING

If the source angle relative to the lens ϕ is larger than θ_E, multiple images of the source will not be formed, but the single image of the source will be elongated. The huge mass associated with clusters of galaxies distorts all the background galaxies many arcminutes from the cluster. Foreground galaxy clusters at redshifts 0.2-0.5 with radial velocity dispersions above 700 km sec^{-1} have sufficient mass density to significantly distort background galaxies of redshift greater than 0.4-1. Lensing preserves the surface brightness and spectrum of the source, so that arcs tend to have the very faint surface brightness and blue color of the faint blue galaxies. An example of both weak and strong lensing is shown in Figures 4 and 5.

1.1. INVERSE PROBLEM: MASS FROM IMAGE DISTORTION

This gravitational lens distortion is quantified using the intensity-weighted second moment of the galaxy image orthogonal and along the radius relative to the lens center (TVW90). A dimensionless scalar alignment T, calculated from these principle axis transformed source ellipticities, is related to the projected mass density clumping and is defined at each point ($\vec{r}$) in the image plane via the (r,θ) principal-axis transformed second moments of the background galaxy image:

$$T(\vec{r}) = \frac{i_{\theta\theta} - i_{rr}}{i_{\theta\theta} + i_{rr}} = \frac{2(1-\kappa)\gamma}{(1-\kappa)^2 + \gamma^2} \simeq \frac{2\gamma(\vec{r})}{1-\kappa(\vec{r})}, \tag{3}$$

where the convergence $\kappa(r) = \Sigma(r)/\Sigma_c$ and the shear $\gamma(r) = [\bar{\Sigma}(r) - \Sigma(r)]/\Sigma_c$, (Miralda-Escudé 1991), and where Σ_c is the critical surface mass density, related to the distance ratio: $\Sigma_c = c^2/(4\pi G D)$. The distance ratio for a foreground-background pair is (cf. Blandford and Narayan 1992)

$$D = \frac{(1 - q_o - d_1 d_2)(d_1 - d_2)}{(1 - q_o - d_2)(1 - d_2)(1 + z_{fg})}, \tag{4}$$

where $d_1 = \sqrt{1 + q_o z_{fg}}$ and $d_2 = \sqrt{1 + q_o z_{bg}}$.

Introducing a galaxy light distribution prior, the tangential second moments are

$$i_{\theta\theta} = M_{20} sin^2\phi + M_{02} cos^2\phi - 2M_{11} sin\phi cos\phi \tag{5}$$

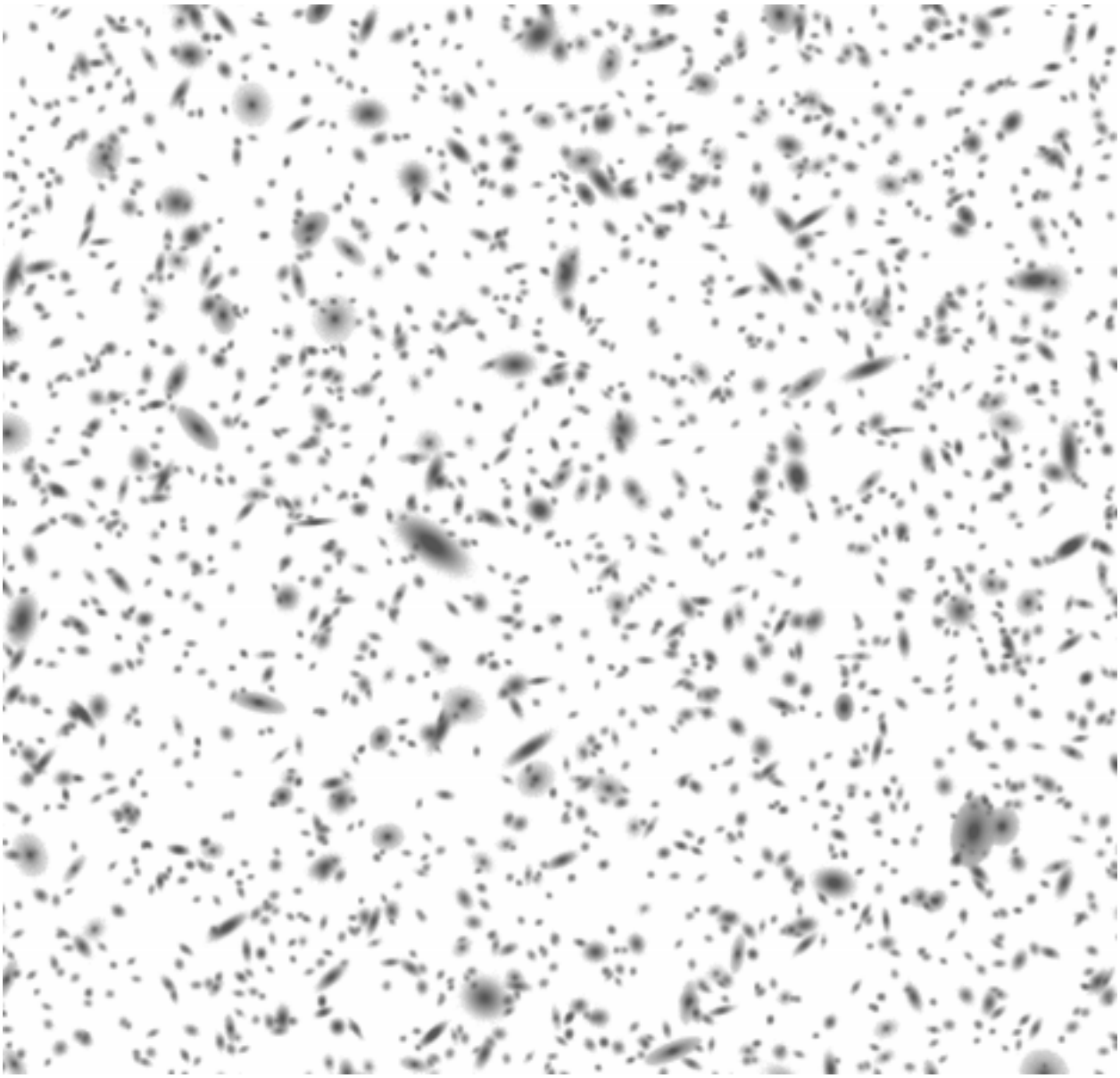

Fig. 4.— *A view of the sky, several arcminutes wide, looking through the forest of galaxies out to redshift 3. This simulation was made to simulate Hubble Space Telescope deep imaging data. No large dark matter concentration was included.*

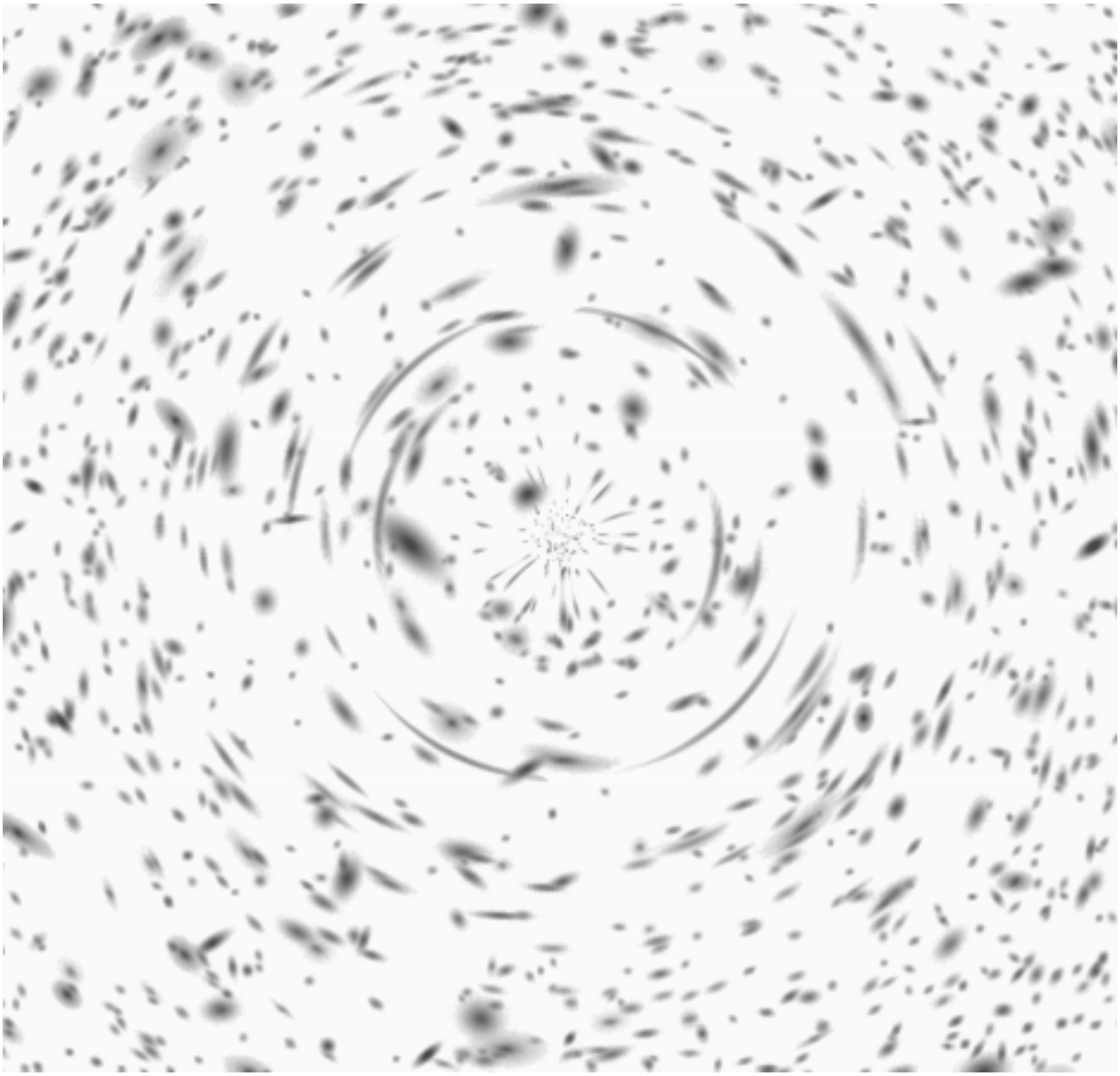

Fig. 5.— *The effects of a dark matter concentration of the type found in rich clusters of galaxies on the simulated sky shown in the previous figure. Foreground galaxies are unaffected; background galaxies are increasingly distorted at higher redshift. Both strong lensing (large arcs, some multiple images of a single source) and weak lensing (mildly distorted single source galaxy image) are seen. The radial spikes close to the center are a diagnostic of a soft mass core.*

$$i_{rr} = M_{20} cos^2\phi + M_{02} sin^2\phi + 2M_{11} sin\phi cos\phi$$

where ϕ is the position angle of the vector from the point (x,y) to the background galaxy, relative to the x-axis. The intensity-weighted second moment $M_{lm,g}$ of background galaxy g is defined by

$$M_{lm,g} \;=\; M_{0,g}^{-1} \int (\delta x)^l \; (\delta y)^m \; W(\delta x, \delta y) \; [I_g(\delta x, \delta y) - I_0] \; dx \; dy, \tag{6}$$

$$M_{0,g} \;=\; \int W(\delta x, \delta y) \; [I_g(\delta x, \delta y) - I_0] \; dx \; dy,$$

where $\delta x = (x - < x >_g)$ and similarly for δy, the sky intensity near this background galaxy is given by I_0, and optimal normalized Gaussian weights $W(\delta x, \delta y, I(x,y))$ are calculated from the half luminosity radius. An unlensed population of galaxies randomly placed and oriented will give a net distortion $T(\vec{r})$ of zero at every point in the image plane, while a population of lensed galaxies will give a positive value at the point corresponding to the lens center.

2. CLUSTER MASS PROFILES AND MAPS FROM ARCLETS

To construct an image of the gravitational lens projected mass distribution, the distortion statistic $T(\vec{r})$ may be computed over a grid of positions as candidate lens centers. In the weak lensing limit it can be shown that the tangential alignment T is a measure of the mass contrast (Tyson, *et al* 1984; Miralda-Escudé 1991):

$$T(\vec{r}) \;=\; 2 \; [\Sigma_{av}(< r) - \Sigma(r)] \; \Sigma_c^{-1}, \tag{8}$$

At any point $\vec{r}$ in the image plane we can sum over the tangential alignment of all source images about that point, creating a continuous scalar distortion statistic $\bar{T}$:

$$\bar{T}(\vec{r}) = \int K(\vec{u}) \; T(\vec{r} - \vec{u}) \; d\vec{u}, \tag{9}$$

where the apodization kernel $K(\vec{u})$ weights source images at large radius less, and is generally of the form $K(\vec{u}) \;=\; (u^2 + u_0^2)^{-1}$. For $\bar{T}$ to be simply related to the mass (Kaiser and Squires 1993) $K(s)$ must asymptotically approach the power law s^{-2} at large s. Since light bending angles from different mass components add, the distortion $\bar{T}$ at any point should be related to

the mass density contrast, if the mass can be represented as a sum of cylindrically symmetric distributions. The solution to this inverse problem for the contrast of the projected lens mass density Σ is then given by a simple integral of the shear over radius from the lens center. The average projected mass density interior to radius r is given by

$$\bar{\Sigma}(r) \;=\; \Sigma_c CB(r) \int_r^{r_{\rm max}} T(r)\; dlogr \;+\; \bar{\Sigma}(r, r_{\rm max}), \tag{10}$$

where C is the seeing correction obtained via simulations, $B(r) = (1 - r^2/r^2_{max})^{-1}$, and $\bar{\Sigma}(r, r_{max})$ is the average density in the annulus between r and $r_{\rm max}$. For a sufficiently large field $\bar{\Sigma}(r, r_{max})$ is small compared with with peak density. This is called "aperture mass densitometry." A radial plot of the projected surface mass density found using Equ 10 is shown in Figure 6 for $z_l = 0.3$, $\sigma_v = 1000$ km sec^{-1} simulations with two different mass profiles.

The distortion image $\bar{T}$(x,y) uniquely locates the lens mass, obtains $M(< r)/r$, and gives its morphological shape on the sky. A useful check of this procedure uses the mass map (Equ 9) as input to a Bayesian search in model mass distribution space, solving for the dark matter mass and core size. For the known source ellipticity distribution, a given source redshift distribution, and a test radial mass distribution model, a maximum likelihood calculation yields the lens M/r (or equivalent velocity dispersion) and core radius. From the inversion of 6000 arclets surrounding the rich z = 0.18 cluster A1689, we found a steeper than isothermal profile beyond 300 h^{-1} kpc radius (Tyson & Fischer 1995). Some clusters at high redshift are nearly as compact in mass. In rich compact clusters mass appears to trace the cluster red light, on scales of a few $\times 100\ h^{-1}$ kpc, with rest-frame V band mass-to-light ratios of a few hundred h in solar units.

The mass core radius is smaller than most observed X-ray core radii in nearby clusters, suggesting that the X-ray gas may be less relaxed dynamically than the dark matter. Over the past decade, theoretical CDM N-body simulation mass core sizes have evolved steadily downwards, past the observed mass cores, towards a singular distribution. In 1990 we reported a (30-50 kpc) mass core radius much smaller than the X-ray core (and then current N-body simulation cores). By 1998 the N-body simulations have high resolution and give mass cores much smaller than our observed mass cores (still 30-40 kpc). At least for rich clusters these lens studies appear to confirm the large mass which was implied by virial calculations using velocity dispersions.

Because faint blue galaxies become more common at redshifts above 0.5, most studies of weak lensing have been confined to lenses around redshift 0.2 – 0.4. However, see Clowe, etal (1998) for a nice example of weak lensing in a couple of clusters at z = 0.8. Figure 7 shows an example of weak lensing reconstruction of mass, with 1st order strong lensing

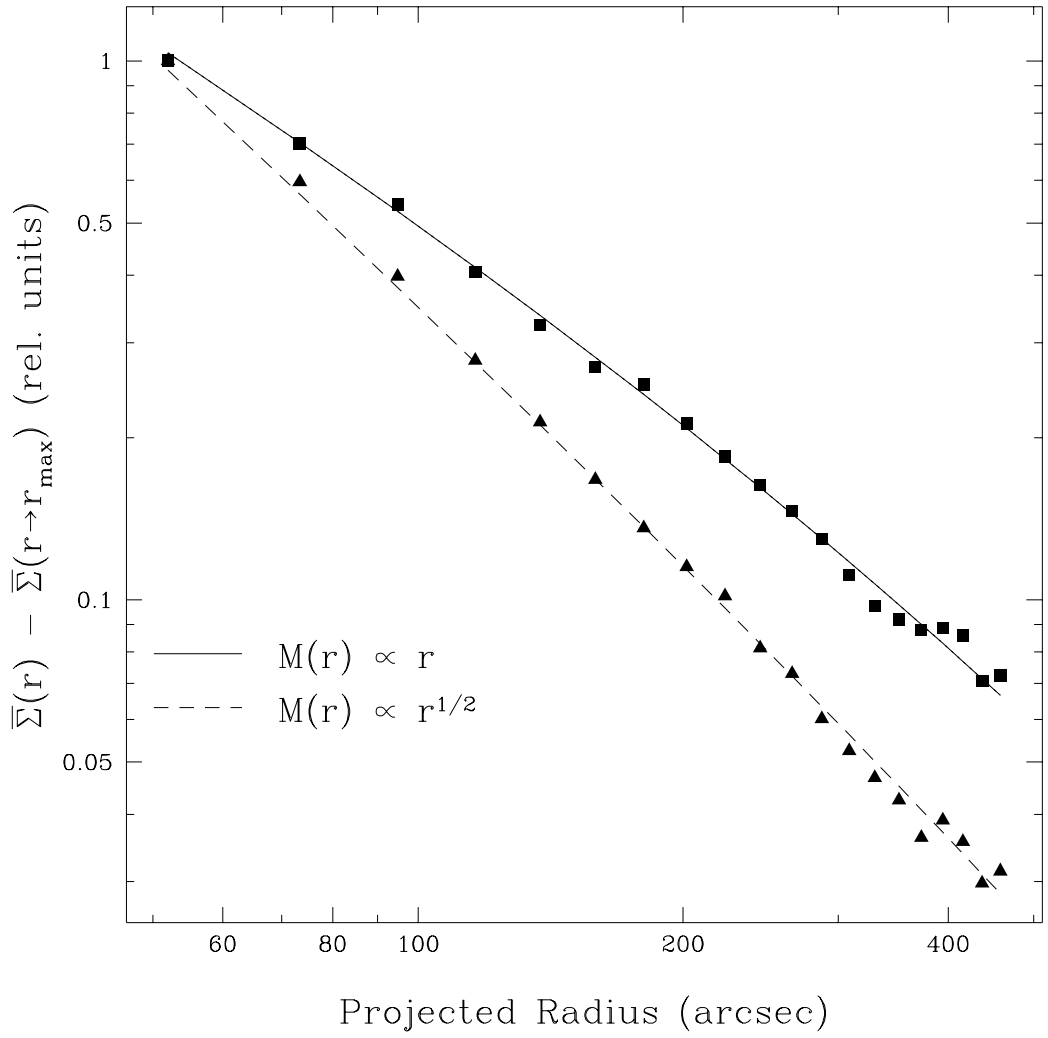

Fig. 6.— *A radial plot of the projected mass density contrast obtained by inversion of the arclets in two 29 B mag arcsec^{-2} noisy simulations of a cluster of galaxies dominated by dark matter with σ_v = 1000 km sec^{-1}. Two mass distributions were used: The lines are the input mass density functions.*

corrections included. See also Squires etal 1997.

3. LARGE SCALE DARK MATTER

By concentrating on the largest luminous structures known, clusters of galaxies, we are biased to radiation. We have in effect been looking under the lamp post for dark matter. Does light trace mass under all conditions? Larger scale applications of this dark matter mapping may eventually find clumped dark matter unrelated to galaxies or clusters of galaxies. Mosaics of CCDs make such a large scale search for coherent alignment in the distant faint galaxies particularly attractive, and dark matter on angular scales up to degrees can in principle be studied in this way. Dark matter may exist in places where there is no current star formation activity. Larger scale applications of this dark matter mapping may eventually find clumped dark matter unrelated to galaxies or clusters of galaxies; I will show a deep image of a good candidate.

If we wish to extract only information on the statistics of the foreground mass overdensities, rather than map them, there is a tensor statistic analogous to the scalar two-point correlation function (Gunn 1967; Valdes, *et al* 1983; Miralda-Escudé 1991; Blandford, *et al* 1991; Seljak 1997). All pairs of galaxies separated by some angle on the sky are summed separately in bins of mutual orientation. This integral tensor statistic called the orientation correlation function (OCF) is then built from these summed orientation data. The OCF has both parallel and orthogonal orientation components, each a function of angle on the sky. The OCF detects an excess over random for background galaxies to be oriented parallel or orthogonal to one another. In this way much larger areas of the sky may be covered and a smaller amplitude statistical mass fluctuation spectrum may be detected.

The observational challenge in low shear measurement is systematic errors due to variations across the detector of the point spread function, optics astigmatism, and variable field distortion due to atmospheric refraction. These systematics can be overcome by chopping and trailing techniques, and optics calibration in rich star fields. Preliminary measurements of the arclet orientation correlation function in random fields yield shear correlations which are below the SCDM prediction. The key in finding the rest of the dark matter, even in places where there are no clusters, is to measure shear over much larger areas. This also means that systematics will have to be controlled at the 0.1-0.5 percent shear level. With Gary Bernstein at U. Michigan, we have built a large area blue-sensitive CCD mosaic camera for the 4-meter Blanco telescope at CTIO. With this instrument we have a chance of viewing mass in ordinary places, rather than in the inner parts of massive rare overdensities.

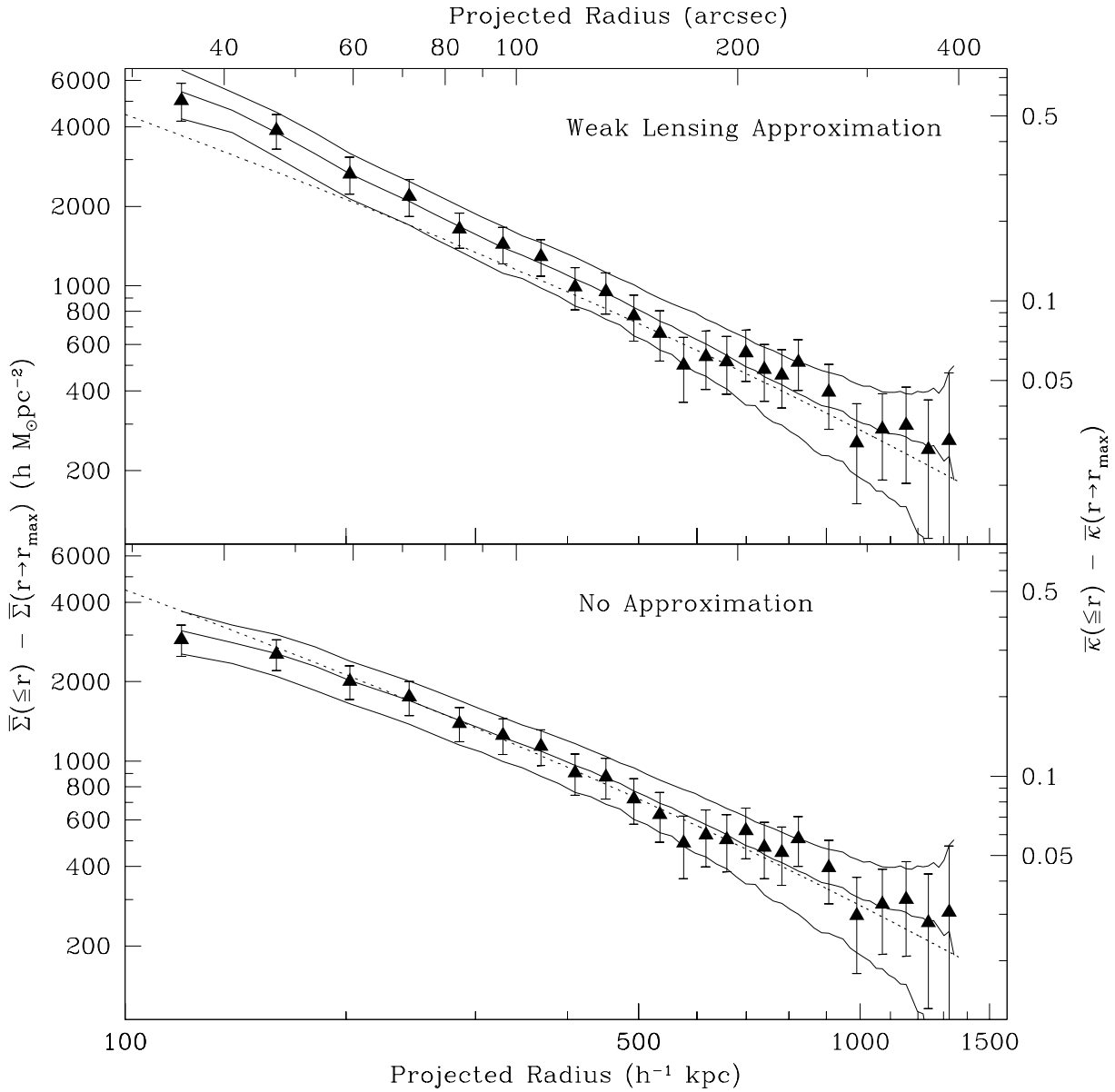

Fig. 7.— *The radial mass distribution of the cluster RXJ1347, with and without strong lensing corrections, as in Equation 3 (Fischer & Tyson 1997). The cluster RXJ 1347.5-1145, at a redshift of* $z = 0.451$*, has an X-ray luminosity* $L_X = 2 \times 10^{46}$ *erg* s^{-1}*.* $\kappa = \Sigma/\Sigma_{crit}$*.*

4. LARGE CCD MOSAIC

The Big Throughput Camera is so named because it was the only operating large mosaic of back-illuminated CCDs, giving it much more throughput than other mosaics with comparable field of view, as well as good blue sensitivity. (See Wittman, etal 1998) [Note: the Sloan CCD mosaic just had its "first light"; this is a much bigger array of the same type of CCDs as the BTC]. The format is a 2×2 array of thinned, broadband antireflection-coated 2048×2048 SITe CCDs. The 4-CCD mosaic covers an 11.7×11.7 cm area. Mounted at the prime focus of the 4-meter Blanco Telescope at CTIO, the 24 micron pixels subtend 0.43 arcsec on the sky, providing a 34.8 arcmin field of view with 5.5 arcmin gaps. Each CCD is separately adjustable in position to $\sim 5\,\mu m$ accuracy and cooled to 170 K.

The BTC's large field of view is ideal for searches for rare objects or events, statistical studies of large numbers of objects, and studies of anything which covers large angular scales. In its year of operation the BTC has been used by a group searching for faint quasars and two groups searching for high-redshift supernovae (twenty discovered per night!), which can be used to constrain fundamental cosmological parameters. For the first time, large numbers of high-redshift supernovae are being discovered: thirty-two identified in first-year BTC images have been confirmed and announced by one team, and a similar number has been found by the other team. A search for Kuiper belt objects is being conducted.

Our studies of large-scale dark matter distribution using weak gravitational lensing exemplify the other two typical uses of the BTC, amassing large-number statistics and covering large angular scales. In weak lensing, the signature of intervening concentrations of dark matter is a small nonrandom component induced in the otherwise random orientations of background galaxies, hence large-number statistics are required. In addition, large angular fields are required to trace the full extent of the dark matter.

We require a large contiguous field of view. The gaps are filled in with "shift-and-stare" exposures, with large shifts of about 1000 pixels (7 arcmin). After about 18 exposures, a contiguous field of 47 arcminutes is covered. The unique problem of large focal-plane mosaics is field distortion, since they cover most of the usable field of view of large telescopes. In the case of the BTC at the Blanco telescope, the prime focus corrector induces a radial distortion of about 60 pixels, or a few percent, at the corners of array. In addition, the corrector lenses over each of the CCDs introduce a small additional distortion, differential refraction over 35 arcmin is significant and constantly changing in direction, atmospheric pressure variations can cause changes in the focal plane scale from exposure to exposure, and the small field rotation caused by the slight polar misalignment of the telescope is evident over this wide a field. Without correction for these effects, multiple shifted exposures cannot be combined

into a single deeper image.

These effects are corrected using a parametric model of the entire optical system and observations of astrometric standard fields from the United States Naval Observatory at a variety of airmasses with each filter used in the observing run. The observed star positions provide constraints on our model of the optical system in which parameters such as the amplitude of the radial distortion and its center relative to the BTC center are allowed to vary. The fit generally converges to a solution with an rms scatter of 0.3 pixels, or 0.13 arcsec. We then apply the model with its best-fit parameters to our science observations, and for some applications such as surveys, tenth-arcsecond accuracy is more than sufficient. However, higher accuracy is required for our gravitational lensing studies. This is because gravitational lensing analyses are based on image shapes, and shapes on a combined frame can be significantly altered if the image positions differ by even a tenth of an arcsecond on the individual frames. Therefore, for each set of images to be combined, we derive an additional third-order polynomial distortion to each exposure by forcing the coordinates of high signal-to-noise objects to agree among exposures. The residuals from this fit are about 0.06 pixels, or 26 milliarcseconds.

In gravitational weak lens shear measurements one must be particularly careful that the point-spread function (PSF) is not systematically out of round. We have found that astigmatism in the telescope optics is the dominant cause of stellar profile ellipticity systematics. We convolve the image with a flux-conserving kernel designed to circularize stellar images. Astigmatism combined with phase diversity across the chips means that the ellipticity and position angle vary with position, so we construct a position-dependent kernel by fitting a fourth-order polynomial function of x and y to the observed moments of those objects which appear to be stellar. The convolution step adds a minimal amount to the stellar image size, on the order of a few percent, while reducing stellar ellipticities by a factor of ten or more, to less than 0.001.

5. COSMIC COMPLEMENTARITY

The observational situation in the $\Lambda - \Omega_M$ plane, mid-1998, is reviewed in Figure 8. Three complementary experiments are plotted. Recently, two groups (The Supernova Cosmology Project and The High-z Supernova Team) using Type Ia supernovae as standard candles (objects of known $\mathcal{L}$) and assuming that their flux measurements (i.e., $\mathcal{F}$) were not contaminated by sample selection, evolution, or dust systematics, both conclude that the expansion of the Universe is accelerating rather than decelerating (i.e., $q_0 < 0$). If correct, this implies that much of the energy in the Universe is in an unknown component. The sim-

plest explanation is a cosmological constant with $\Omega_\Lambda \sim 2/3$. My estimate of the likelihood contours are shown.

The pattern of anisotropy in the CMB depends upon the total energy density in the Universe. The first acoustic peak in the multipole power spectrum is $l_{\rm peak} \simeq 200/\sqrt{\Omega_M + \Omega_\Lambda}$. These current likelihood contours are shown as dashes. The CMB anisotropy does not measure mass at z=1000 directly; a model relating three mass-derived effects on the radiation must be fit to the CMB anisotropy data. Note that likelihood contours for these first two experiments are roughly orthogonal; as the new generation of satellite CMB observations map out the fine scale structure of the microwave sky, the position our Universe occupies in this plane will be strongly constrained.

Finally, as direct lensing observations of dark matter explore more of the Universe, the vertical bar "known matter" will move to the right. It will be interesting, and a test of our cosmological model, if all three are consistent. Such a dark matter survey is feasible, using current technology.

6. DARK MATTER TELESCOPE

A definitive measure of the overdensity spectrum of the dark matter on 10 Mpc scales is technically within reach. Deep imaging of hundreds of thousands of distant galaxies at several wavelengths – to get statistical redshifts from their colors – repeated in many different directions, would have the precision to detect 10 percent of the statistical weak lensing shear predicted by standard CDM theory. An accurate measurement in twenty two-degree areas of the sky – to get the cosmic variance – would provide a direct measure of Ω_M and the mass fluctuation spectral index. With a dedicated 4 or 5-meter "Dark Matter Telescope", an advanced mosaic of 32 CCDs covering over half a degree, and deep imaging in 4 wavelength bands, this project would take five years to complete. The payoff in our understanding of dark matter and cosmology would be worth the effort.

Acknowledgements: My principal collaborators in this research are Gary Bernstein, Ian Dell'Antonio, Phil Fischer, Raja Guhathakurta, Ayana Holloway, Greg Kochanski, Jordi Miralda-Escudé, and Dave Wittman.

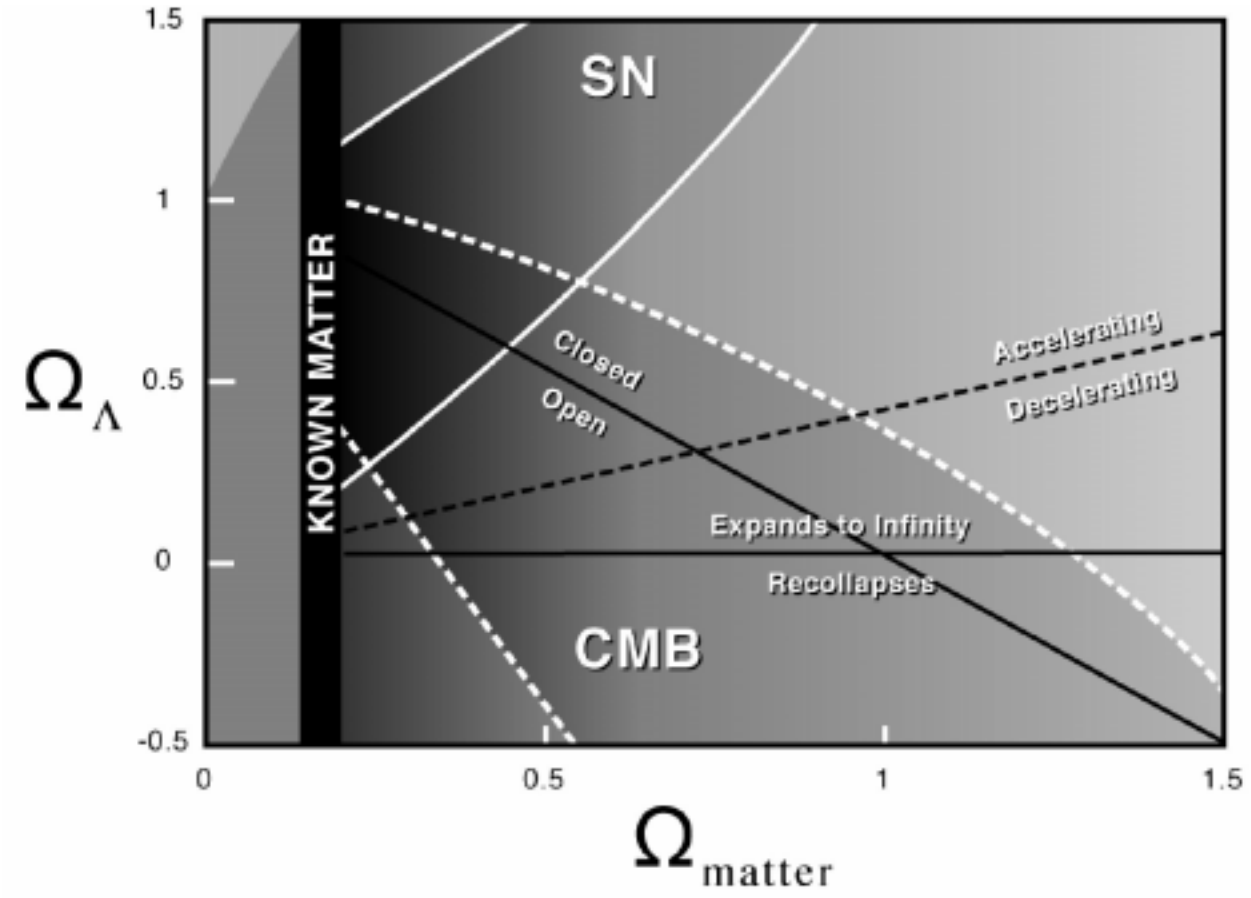

Fig. 8.— *The current situation in the cosmological constant – matter plane. Three key experiments are indicated: Supernova measurements of the acceleration (SN), cosmic microwave background anisotropy measurements (CMB), and direct measurements of mass (shading). All three will see vastly decreased errors in the next few years. The "known matter" is a lower limit based on extrapolating cluster masses to the field, assuming idential M/L ratios. As more mass is found this vertical black bar will move to the right. Note that the recent determination of the cosmic abundance of deuterium suggests* $\Omega_{matter} = 0.4$.

REFERENCES

Blandford, R.D. & R. Narayan 1992, Ann. Rev. Astron. Astrophys, 311.

Blandford, R.D., A.B. Saust, T. Brainerd, & J.V. Villumsen 1991, Mon. Not. Royal Astron. Soc. 251, 600.

Blumenthal, G, Faber, S., Primack, J. & Rees, M. 1984, Nature 311, 517.

Burles, S. and D. Tytler, 1997, astro-ph/9712265.

Carlberg, R. G., H. K. C. Lee, E. Ellington, R. Abraham, P. Gravel, S. Morris, and C. J. Pritchet, 1996, Astrophys. J. 462, 32.

Clowe, D., Kaiser, N., Luppino, G., Henry, J.P., & Gioia, I.M. 1998, astro-ph/9801208.

Colley, W.N., J.A. Tyson and E.L. Turner 1996, ApJL 461, 83.

Evrard, A. E., etal., 1996, Astrophys. J. 469, 474.

Fischer, P., & Tyson, J.A. 1997, AJ, 114,14.

Garnavich, etal. 1998, ApJ 493, 53.

Grossman, S. A. & R. Narayan 1988, ApJL 324, 37.

Gunn, J.E. 1967, ApJ 147, 61.

Im, M., S. Casertano, R.E. Griffiths, K.U. Ratnatunga, & J.A. Tyson 1995, Astrophys. J. 441, 494.

Kaiser, N. & G. Squires 1993, ApJL 404, 441.

Miralda-Escudé, J. 1991a ApJ 370, 1.

Peebles, P. J. E., 1993, *Principles of Physical Cosmology* (Princeton University Press).

Press, W. & Gunn, J.E. 1973, ApJ, 185, 397.

Syer,, D. & White, S.D.M. 1998, MNRAS 293, 337.

Schneider, P., Ehlers, J., & Falco, E.E., 1993, "Gravitational Lenses" (Springer, NY), 244

Squires, G. etal 1997, ApJ 482, 648.

Seljak, U. astro-ph/9811124.

Turner, E.L., J.P. Ostriker, & J.R. Gott 1984, Astrophys. J. 284, 1.

Tyson, J.A., Kochanski, G., & Dell'Antonio, I.P. 1998, ApJL 498, 107.

Tyson, J.A. & P. Fischer 1995, ApJL 446, 55.

Tyson, J.A., Valdes, F., & Wenk, R.A. 1990, ApJL, 349, L1

Tyson, J.A., F. Valdes, J.F. Jarvis, & A.P. Mills 1984, ApJL 281, 59.

Valdes, F., J.A. Tyson, & J.F. Jarvis 1983, ApJ 271, 431.

White, S.D.M., Frenk, C., & Davis, M. 1983, ApJ 274, L1.

Wittman, D. etal. 1998, SPIE, 3355, 626.